applied sciences

MDPI

Article

Experimental Study on Mechanical Deformation and Energy Evolution of Deep Coal Under Complex Stress Paths

Yue Jiang [1,2], Xingfeng Mao [2], Dongming Zhang [2] and Xiang Yang [2,*]

[1] School of Information Engineering, Jiangxi University of Science and Technology, Ganzhou 341000, China; 6720221154@mail.jxust.edu.cn
[2] School of Emergency Management and Safety Engineering, Jiangxi University of Science and Technology, Ganzhou 341000, China; 18281573181@163.com (X.M.)
* Correspondence: march1714132497@163.com

Abstract: This study proposes a novel cyclic stress path with simultaneous axial and confining stress and conducts triaxial testing on raw coal over various cycle periods. The analysis of bias stress–strain curves, deformation parameters, and energy indexes elucidated the mechanical and energy evolution patterns of coals under novel stress routes. The three deformation parameters can well reflect the deformation characteristics of the specimens. The last few cycles saw an increase in Poisson's ratio and irreversible deformation, indicating that the coal samples were likely to crack. Specimens are more prone to instability and destruction due to increased expansion under high frequency loading. To explore the energy evolution, the energy percentage and damping ratio are added to the previously mentioned basic energy indexes. Faster cyclic period reduces specimen microstructure stability, increases mineral particle misalignment friction, and raises dissipated energy percentage and damping ratio. D_S and D_d based on deformation parameters and cumulative dissipated energy, respectively, can characterize the coal's three damage stages of "deceleration–stabilization–acceleration". Both damage variables accumulate faster in the acceleration damage stage due to cyclic period acceleration.

Keywords: cyclic loading and unloading; different cyclic periods; deformation characteristics; energy evolution; damage variable

check for updates

Academic Editor: Alberto Campagnolo

Received: 21 January 2025
Revised: 11 February 2025
Accepted: 17 February 2025
Published: 18 February 2025

Citation: Jiang, Y.; Mao, X.; Zhang, D.; Yang, X. Experimental Study on Mechanical Deformation and Energy Evolution of Deep Coal Under Complex Stress Paths. *Appl. Sci.* **2025**, *15*, 2167. https://doi.org/10.3390/app15042167

Copyright: © 2025 by the authors. Licensee MDPI, Basel, Switzerland. This article is an open access article distributed under the terms and conditions of the Creative Commons Attribution (CC BY) license (https://creativecommons.org/licenses/by/4.0/).

1. Introduction

The mining process in deep mines encounters severe conditions characterized by "high geo-stress, high temperature and high osmotic pressure" [1–3]. The disruptive impact of repeated loads, such as construction blasting and face mining, disrupts the natural equilibrium of coal resources. This alteration affects the strength, deformation, and damage characteristics of the coal body, making it susceptible to dynamic disaster incidents related to the destabilization and destruction of coal rock. Consequently, this poses a significant risk to the safe mining operations in coal mines [4–6]. The mechanical behavior and energy characteristics of raw coal under cyclic loading conditions differ from those observed under conventional stress conditions. Therefore, it is essential to investigate the deformation damage and energy evolution patterns of the coal body subjected to cyclic loading with varying cyclic periods.

Rocks exhibit diverse mechanical behaviors and damage patterns when subjected to various dynamic loads [7–9]. Wei [10–12] studied the deformation characteristics and damage features of fracture-containing rocks under uniaxial and triaxial cyclic loading and pointed out that localized damage and deformation occur during the unloading of

confining stress. Additionally, radial and volumetric strains increase significantly, the deformation modulus initially rises and then declines, and Poisson's ratio continuously increases. Dang [13–15] conducted triaxial cyclic loading and unloading compression tests on sandstones subjected to varying upper limit axial stresses. This research revealed the rules of damage evolution, life prediction, and the damage mechanisms of sandstones. Ren [16,17] used conventional and cyclic triaxial dynamic load tests at various frequencies on coal rock under high stress to investigate the damage mechanisms and the laws governing strength deterioration of coal rock induced by dynamic loading. Chen [18] analyzed the mechanical properties and crack extension behavior of sandstone through a series of triaxial experiments and proposed a damage variable based on crack evolution. Duan and Gong [19,20] investigated the deformation characteristics of coal samples under various cyclic loading and unloading stress paths. They established the evolution law of damage variables based on the loading and unloading response ratio. The elastic modulus and Poisson's ratio of the rock during variable amplitude loading exhibit a nonlinear decrease and increase, respectively, in relation to the loading rate, and show a negative correlation with the stress amplitude [21]. The stress paths utilized in the aforementioned studies primarily involve cyclic variations in confining stress or axial stress alone. There is a scarcity of experimental research examining the cyclic loading and unloading of rocks while simultaneously altering both axial and confining stress. Consequently, there is a significant gap in the literature regarding the impact of cyclic periods on the deformation properties of rocks under conditions of simultaneous changes in axial and confining stress.

The deformation damage of rock is a process that progresses from local rupture to partial destruction and ultimately to complete crushing and destabilization, this process is accompanied by energy input, accumulation, and dissipation. In essence, rock damage is fundamentally an energy-driven process of destabilization and destruction [22–25]. Currently, many scholars have sought to understand the behavior of rock during cyclic loading and unloading from an energy perspective. However, most of their research has concentrated on uniaxial and conventional triaxial experimental methods [26–28]. Li [22] performed uniaxial cyclic loading and unloading tests on coal samples at various loading rates and analyzed the interaction mechanisms of input, elastic, and dissipated energies at each stage, as well as their correlations with loading rates. Additionally, they described the differences in energy conversion at each stage. Song [29] investigated the impact of water content on the damage and energy dissipation characteristics of coal bodies through uniaxial cyclic loading and unloading tests. He [30] explored the linear relationship between the dissipated energy coefficient and both the yield and peak strengths by conducting uniaxial compression tests on various types of rocks. In addition, some researchers have examined the energy evolution of rocks under triaxial cyclic loading conditions. Zhang [31] investigated the energy characteristics of marble under triaxial loading and unloading conditions, deriving the influence of confining stress and unloading rate on the energy evolution of rock samples. Jiang [32,33] experimented triaxial variable upper and lower limit equal amplitude cyclic loading and unloading of natural state shale under different confining stresses and found that the stresses reaching the energy weakening stage at low confining stresses are lower than those at high confining stresses, while the stresses reaching the energy strengthening stage are higher than those at high confining stresses. Meng [34] conducted triaxial cyclic loading and unloading tests on rock samples under six different confining stresses. The authors proposed a method for calculating rock energy based on the areas of the loading and unloading curves and employed characteristic energy density to characterize the energy evolution behavior of loaded rock samples, thereby elucidating the energy evolution process and the distribution pattern of the confining stress effect. Rock energy evolution under complex cyclic loading needs additional study; however, most

studies focus on input, dissipation, and elastic energy rather than energy percentages and damping coefficient.

This work provides a stress path that transcends prior research' unidirectional cycling, presenting a graded multiple-cycle loading and unloading stress path that integrates simultaneous fluctuations in axial and confining stress. Analyzing deformation parameters, including elastic modulus, Poisson's ratio, and irreversible deformation, alongside energy indices such as energy percentage and damping ratio, elucidates the mechanical response and energy evolution patterns of coal during this stress perturbation process. Two damage variables that reflect the development of coal damage were calculated from both deformation and energy perspectives. Additionally, the effects of the cyclic period on coal samples were compared in terms of deformation and energy. This study offers a theoretical foundation for a deeper understanding of the mechanical response, energy conversion, and damage deterioration mechanisms of coal under dynamic loading. Additionally, it holds significant reference value for evaluating the safety of coal bodies and predicting power-related disasters during the coal mining process.

2. Experimental Preparation and Program

2.1. Specimen Preparation

The specimens used in the test were obtained from the Shenmu Coal Mine in Yulin City, Shaanxi Province, and were processed into standard cylindrical specimens with dimensions of φ50 mm × 100 mm, in accordance with the requirements outlined in the Standard for Testing Methods of Engineering Rock. The non-parallelism of the end faces is limited to 0.02 mm. Given that the coal samples possess an exceptionally high degree of primary cleavage, specimens of comparable quality and surface cleavage characteristics were evaluated and selected for testing.

2.2. Test Equipment

The test was carried out by the self-developed servo test system KDSZS-II. The test system mainly consists of four parts, as shown in Figure 1.

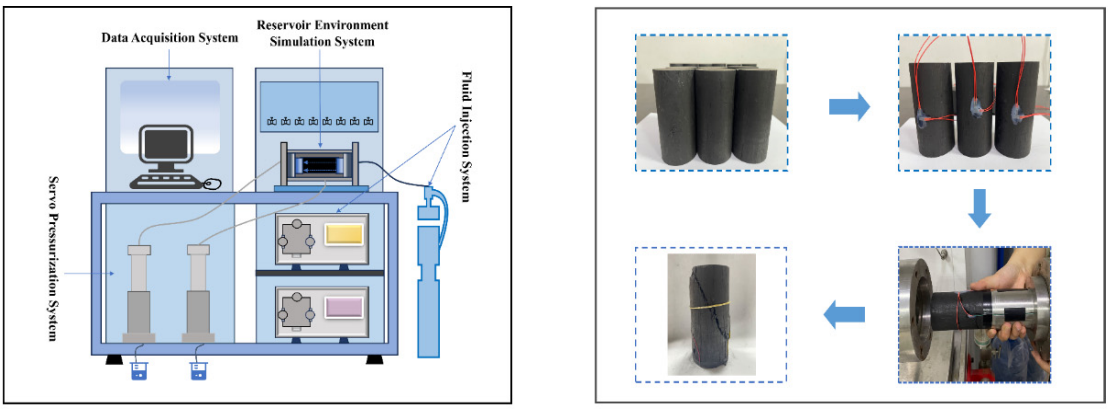


Figure 1. Test equipment and test procedure.

2.3. Test Scheme

In this paper, the tests were carried out according to the following steps:

1. Place the coal sample, with the strain gauges attached, into the gripper for preheating. After installing the three-axis compressor, check to ensure that both the strain gauge and flow meter are functioning properly.

2. Adopt a stress control method by applying axial pressure and confining stress at a rate of 2.8 MPa/min. Gradually increase these pressures until reaching the hydrostatic pressure value. Once the pressure stabilizes, apply a constant gas pressure of 2 MPa and maintain this pressure until the specimen reaches adsorption equilibrium.
3. Cyclic loading and unloading were conducted according to the established cyclic period. Each stage of the cycle was performed six times, with the upper and lower limits of the axial pressure in each stage increasing by an equal amount of 7 MPa. Simultaneously, the upper and lower limits of the confining stress decreased by an equal amount of 6 MPa. This cyclic process continued in stages until the specimen was crushed. The specific stress path is illustrated in Figure 2.
4. The damaged specimen was removed from the rubber sleeve and photographed. It was then replaced with a new specimen for the loading and unloading test. Three sets of the same test were conducted under each cyclic period.

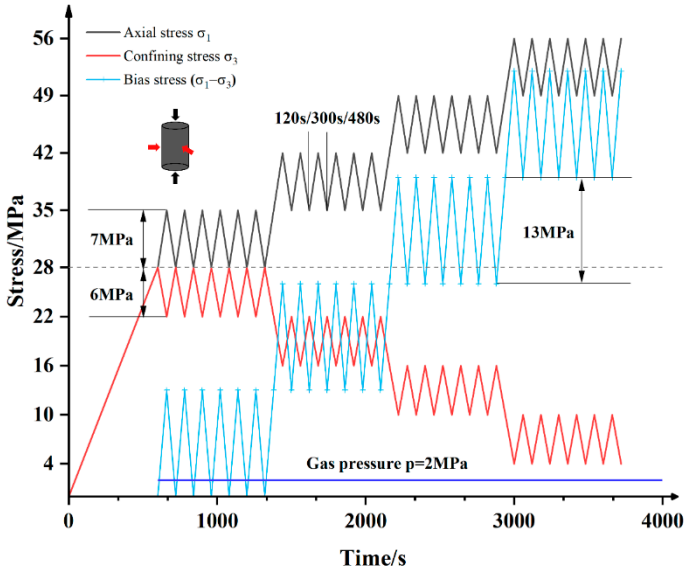


Figure 2. Stress path program.

3. Analysis of Test Results

Figure 3 illustrates the stress–strain curves for various cyclic periods. It is evident that the stress–strain curves create a hysteresis loop in each cycle. This hysteresis loop accurately delineates the plastic deformation caused by the opening and closing of rock fissures. The stress–strain response of the specimens remains rather uniform throughout each cyclic phase. The hysteresis loop area diminishes at all stress levels as it spirals towards the direction of escalating strain with each successive cycle. The irreversible deformations induced by these cycles exhibit less variability, with the exception of the initial cycle, which produces a markedly greater irreversible deformation. This phenomenon largely arises because the escalation of bias stress induces the initiation and propagation of cracks inside the coal samples, leading to considerable plastic deformation. Subsequently, due to the compaction effect, the extent of damage incurred during each cycle is diminished. These data indicate that the rock damage caused by elevated bias stress is far more than the fatigue damage from cyclic loading.

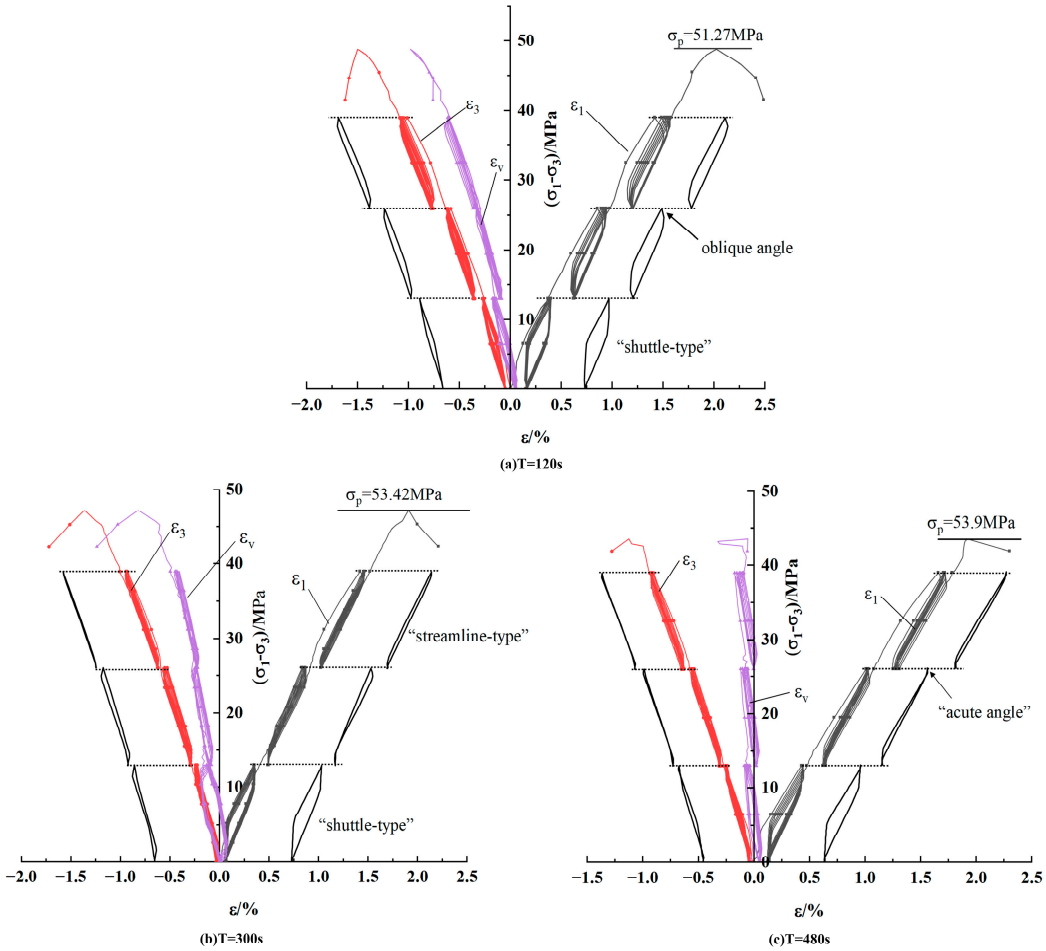


Figure 3. Stress–strain curves at different cyclic periods.

As the stress level increases, the strain span of axial and radial strains increases, and the loading and unloading curves of the hysteresis loop to converge gradually. The configuration of the axial hysteresis loop at stress level 1 is characterized as "shuttle" type (in Figure 3). This phenomenon occurs because when the bias stress level in the loading section is low (about $(\sigma_1 - \sigma_3) < 5$ MPa), the axial stress does not effectively promote the development of internal fissures and the confining stress predominantly restricts the coal samples, leading to a gradual response of axial strain as the bias stress increases. As stress levels increase, the axial hysteresis loop transforms into an extended "streamline" configuration. The configuration of the radial hysteresis loop resembles a "streamline" form, demonstrating a more distinct linearity, which indicates that the radial deformation predominantly occurs as elastic deformation. Further observations revealed that as the cyclic period increases, the angle of the stress–strain curve at the beginning of the unloading of the bias stress at the same level decreases, gradually changing from an obtuse angle to an acute angle, combined with the hysteresis effect, the "obtuse angle" reflects the sluggish strain feedback and rapid plastic deformation response of the coal sample when the bias stress unloading, "acute angle" reflects that the coal sample is sensitive at the bias stress unloading point, with a rapid response to elastic deformation. It indicates that a shorter cyclic period leads to a reduced elastic response and an increased sensitivity to plastic deformation in the coal samples at the peak of the cycle.

Figure 4 shows the bias stress–volume–strain curves of the third cycle in the extraction of each stress level. Volume strain is the combined response of axial and radial strains, which characterizes the overall deformation of the coal sample, $\varepsilon_v = \varepsilon_1 + 2\varepsilon_3$. The coal

sample undergoes shear inflation followed by shear compression during each cycle. The bias stress–volume–strain curves are roughly centrosymmetric along the axis of the line connecting the cyclic onset and peak points, and the overall phenomenon demonstrates a clear expansion and dilation. As stress levels escalate, the spectrum of volume strain values diminishes and moves towards deformation expansion, mostly due to the rise in shear stress. The key point of bias stress at the initiation of specimen shear compression was noted to be progressively nearing the peak stress point of the cycle. Comparing different cyclic periods at the same stress level, as the cyclic period decreases, the volume strain of the specimen gradually shifts to the right, indicating deformed compression. Additionally, the critical point of the bias stress, which transitions from shear inflation to shear compression, gradually decreases. The results indicate that under identical stress conditions, decreasing the cyclic period will make the specimen more susceptible to shear shrinkage, reduce the degree of specimen expansion, and enhance the stability of the overall internal structure of the specimen.

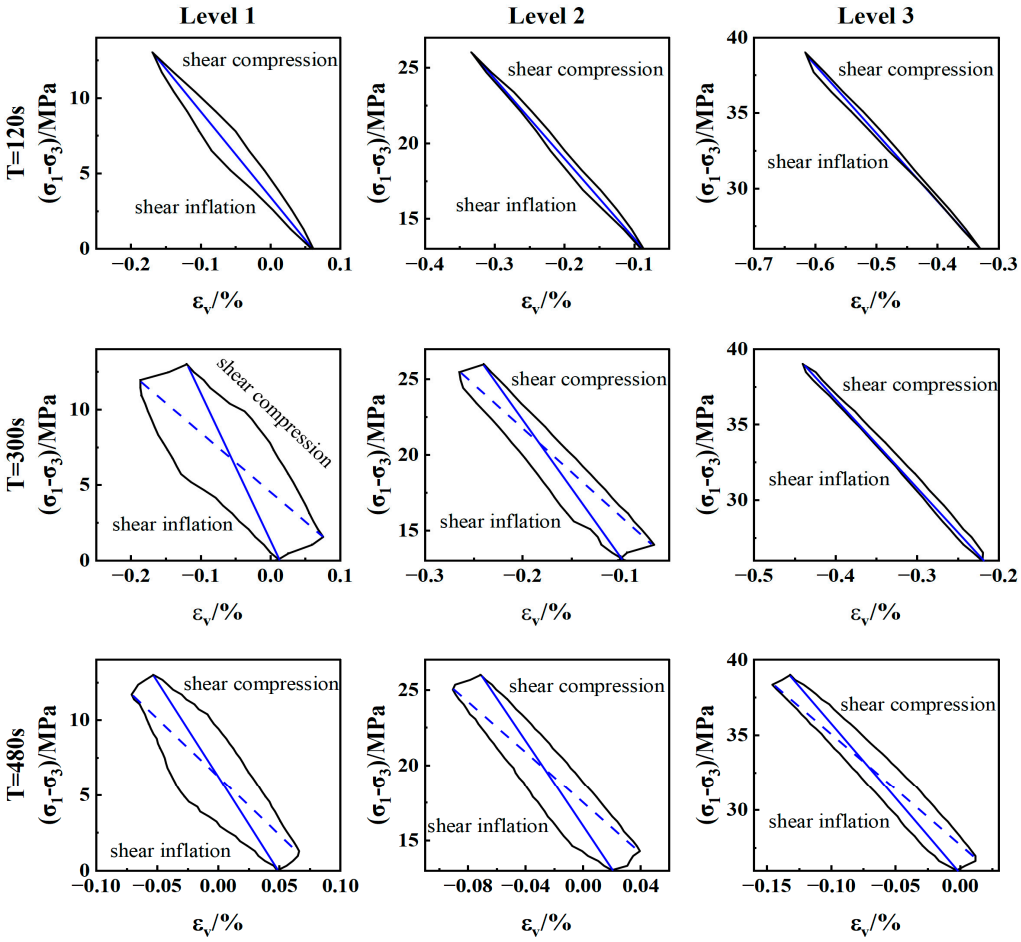


Figure 4. Bias stress–volume–strain curves.

4. Deformation Characteristics

4.1. Elastic Modulus

The elastic modulus E is a crucial parameter that reflects the deformation characteristics of rock. It is important to consider that the coal sample is influenced by gas pressure during the testing process, the axial effective stress σ_1' and radial effective stress $\sigma_2' = \sigma_3'$ are calculated according to the principle of effective stress, and the equations are, respectively [35],

$$\sigma_1' = \sigma_1 - p_1 \quad (1)$$

$$\sigma_2' = \sigma_3' = \sigma_3 - \frac{1}{2}(p_1 + p_2) \tag{2}$$

In the formula, σ_1 and σ_3 are the axial and radial stresses, respectively, and p_1 and p_2 are the inlet gas pressure and outlet gas pressure, respectively.

The elastic modulus of rock during triaxial cyclic loading and unloading is calculated as follows [19]:

$$E = \frac{(\Delta\sigma_1' + 2\Delta\sigma_3')(\Delta\sigma_1' - \Delta\sigma_3')}{\Delta\sigma_3'(\Delta\varepsilon_1 - 2\Delta\varepsilon_3) + \Delta\sigma_1'\Delta\varepsilon_1} \tag{3}$$

In the formula, $\Delta\sigma_1'$ and $\Delta\varepsilon_1$ are the axial effective stress increment and axial strain increment in the elastic interval of bias stress loading/unloading section, and $\Delta\sigma_3'$ and $\Delta\varepsilon_3$ are the radial effective stress increment and radial strain increment in the elastic interval of bias stress loading/unloading section, respectively.

The variation pattern of the elastic modulus is illustrated in Figure 5. Generally, the elastic modulus during the bias stress unloading phase is higher than that during the loading phase. With regard to the overall stress level, the elastic modulus shows a decreasing trend as the stress level increases. For instance, when the cyclic period is 120 s, the average loaded elastic modulus at each stress level is 2.07 GPa, 1.80 GPa, and 1.51 GPa, respectively. This is due to the combined influence of increased shear stress, the development and propagation of internal cracks are intensified, leading to a deterioration in the coal samples' resistance to deformation. The pattern of elastic modulus at the same stress level can be attributed to the internal hardening and softening reactions of the coal samples. From Figure 5, it can be found that at stress level 1, the elastic modulus increases with the number of cycles. This is mainly due to the compaction and closure of the pores and cracks within the coal sample, as well as the filling and compaction of the detrital particles which act as a hardening effect. At stress level 2, the elastic modulus curve takes on a groove shape. This likely occurs because the new formed fissure structure has not yet stabilized as to the next stress level, over time, the particles and cracks gradually adjust and stabilize, the elastic modulus stabilizes or even increases slightly. At stress level 3, the bias stress is further increased, leading to the extension and connection of internal cracks. The weakening effect becomes predominant, resulting in a gradual decrease in specimen stiffness and elastic modulus as the number of cycles increases.

Figure 5 demonstrates a clear upward trend in the elastic modulus curve as the cyclic period increases. Figure 6 illustrates that the average elastic modulus increases as the cyclic period slows down at each stress level. As observed at stress level 1, the average loading elastic modulus during cyclic periods of 120 s, 300 s, and 480 s were 2.07 GPa, 2.17 GPa, and 2.30 GPa, reflecting increases of 4.83% and 10.60%, respectively. The results indicate that an increase in the acceleration of the cyclic period reduces the stiffness of the coal samples, diminishes their ability to withstand external deformation, and renders the samples more vulnerable to destabilizing damage. This can be ascribed to the enhanced formation and proliferation of joint cracks in the specimens, which is intensified by the heightened frictional slide among particles in the coal sample resulting from the accelerated loading rate. In addition, the average increment of elastic modulus of the loaded section at stress level 1 becomes more pronounced as the cyclic period increases, with average increments of 1.65%, 2.41%, and 4.25% at T = 120 s, 300 s, and 480 s, respectively. This may be attributed to the fact that a faster loading rate leads to insufficient engagement friction during the initial loading phase.

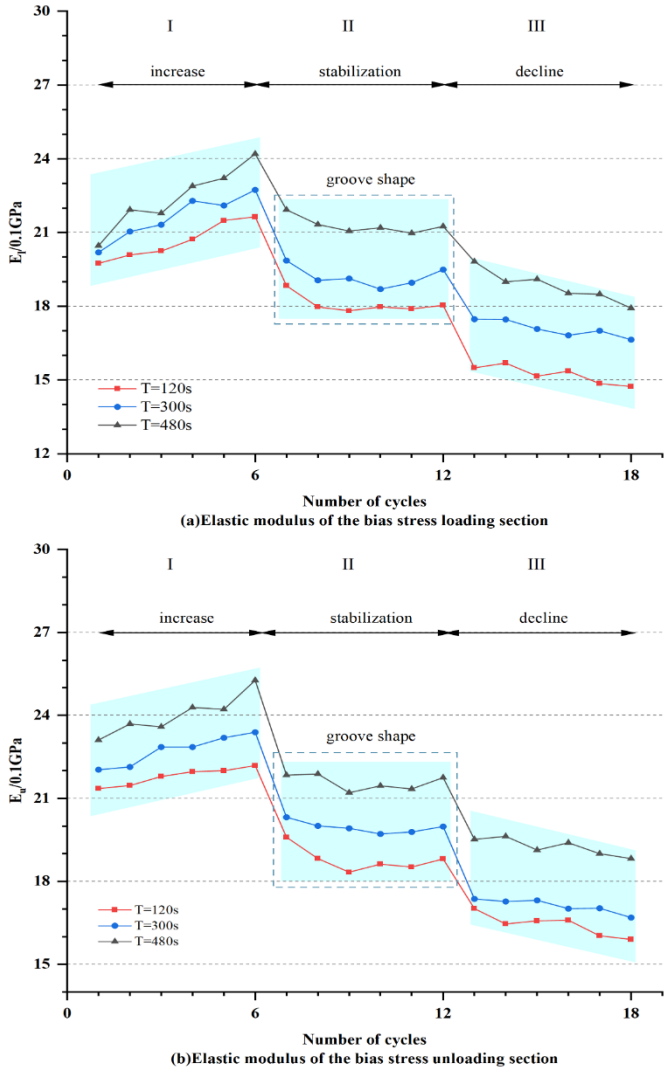


Figure 5. Relationship of elastic modulus with number of cycles.

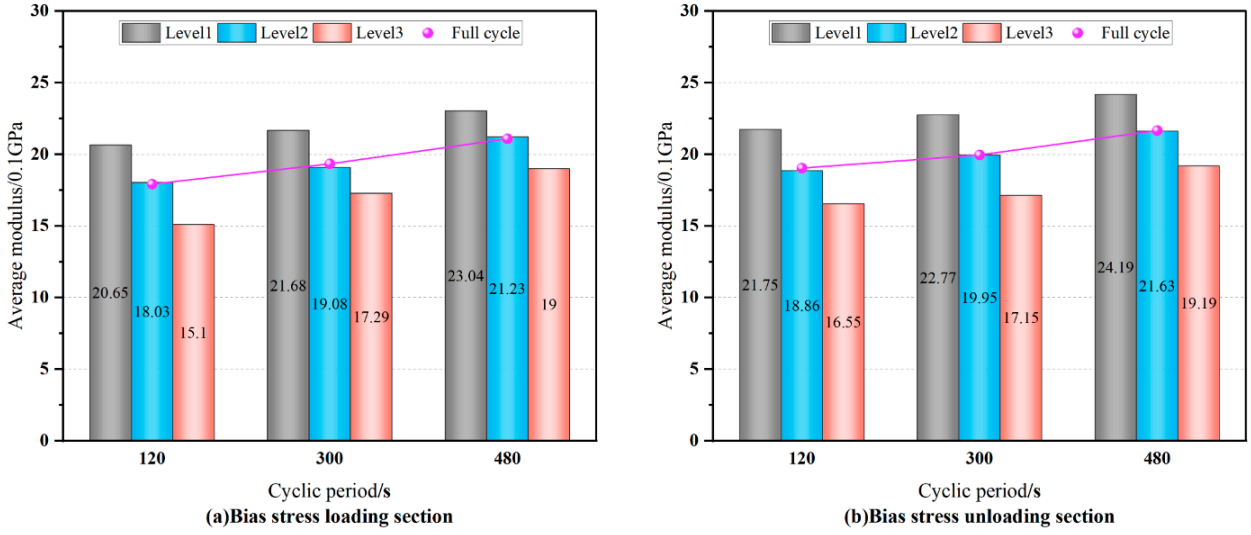


Figure 6. Elastic modulus at different cyclic periods.

4.2. Poisson's Ratio

Poisson's ratio μ is a parameter reflecting the relative deformation of radial and axial directions of the rock in the progressive destruction process of cyclic loading, and the

Poisson's ratio μ_l for the bias stress loading section and the Poisson's ratio μ_u for the unloading section are calculated by the formula [28]:

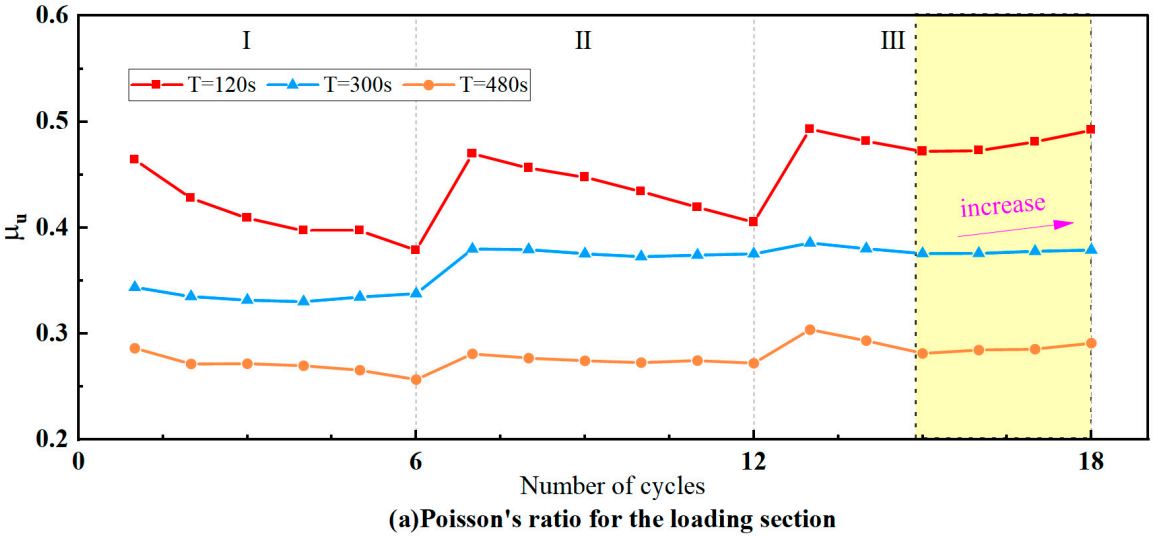
$$\mu_l = (\varepsilon_{3,l} - \varepsilon'_{3,l})/(\varepsilon_{1,l} - \varepsilon'_{1,l}) \quad (4)$$

$$\mu_u = (\varepsilon_{3,u} - \varepsilon'_{3,u})/(\varepsilon_{1,u} - \varepsilon'_{1,u}) \quad (5)$$

where $\varepsilon_{1,l}$, $\varepsilon'_{1,l}$, $\varepsilon_{3,l}$, and $\varepsilon'_{3,l}$ are the axial and radial strains in the elastic interval of the biased stress loading section, respectively, and $\varepsilon_{1,u}$, $\varepsilon'_{1,u}$, $\varepsilon_{3,u}$, and $\varepsilon'_{3,u}$ are the axial and radial strains in the elastic interval of the biased stress unloading section, respectively.

From Figure 7, it can be noticed that the Poisson's ratio of the loaded section is greater than that of the unloaded section. Poisson's ratio increases in a generally stepwise manner as stress levels rise. This behavior indicates that radial deformation becomes more sensitive compared to axial deformation. Under the same stress level, the ductility of the specimen is somewhat limited in the first two levels. This limitation occurs because most of the pores and defects tend to be compressed and filled. In stress level 3, the stress is approaching the yield threshold of the coal samples. The previous cycles of loading and unloading have caused some degree of damage to the specimens, leading to the expansion and development of both new and old cracks. As a result, the radial deformation becomes more pronounced, and the decreasing trend of Poisson's ratio is effectively mitigated. A sustained increase in the Poisson's ratio over three to four cycles, occurring near the time of damage, can serve as a precursor to the rupture of the specimen.

From Figure 7, it can be found that deceleration of the cycle period significantly constrains the Poisson's ratio and mitigates the radial expansion deformation of the specimen. The average Poisson's ratio for each stress level is shown to decrease with the increased cyclic period in Figure 8. In the full process cycle, the average Poisson's ratio of the loading section at T = 120 s, 300 s, and 480 s is 0.45, 0.38, and 0.29, respectively, which decreases by 15.56% and 23.68% in that order. This may be related to the fact that higher loading rates generate greater kinetic energy, leading to increased slip misalignment between the contact surfaces of the coal sample fissures and thus the more pronounced radial deformation.



(a)Poisson's ratio for the loading section

Figure 7. *Cont.*

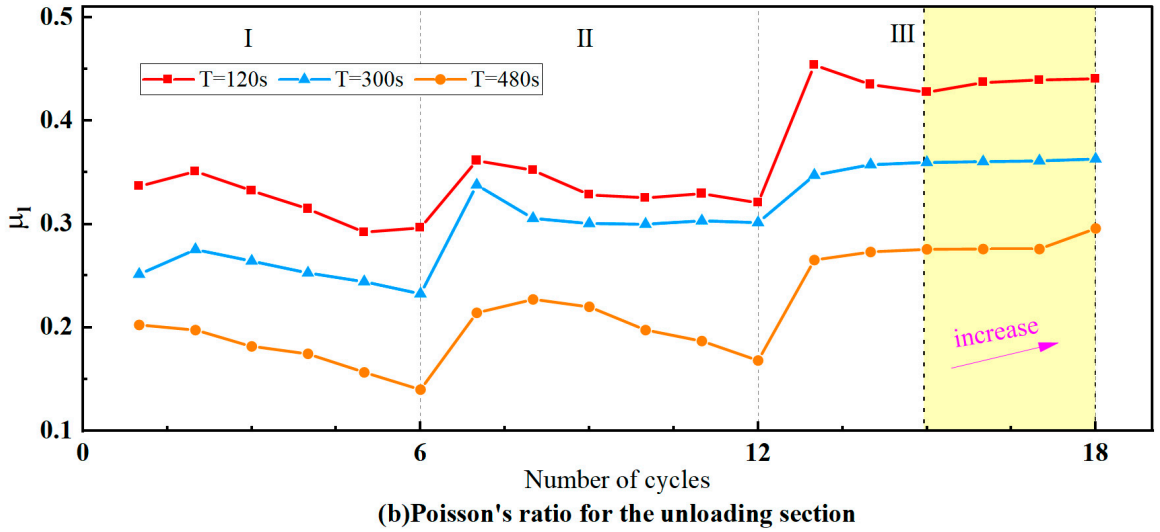


Figure 7. Poisson's ratio versus number of cycles.

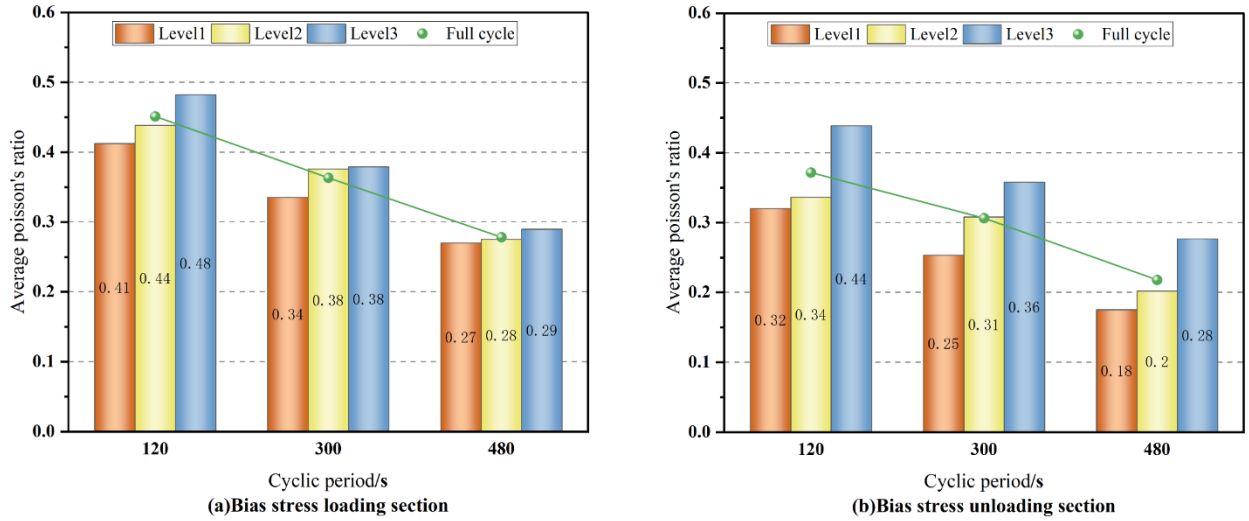


Figure 8. Poisson's ratio at different cyclic periods.

4.3. Irreversible Deformation

Coal samples under cyclic loading and unloading produce axial and radial irreversible plastic deformations, $\varepsilon_{p,1}$ and $\varepsilon_{p,3}$. The total irreversible deformation produced by each cycle is $\varepsilon_p = \varepsilon_{p,1} + 2\varepsilon_{p,3}$. The change pattern is shown in Figure 9. Irreversible deformation escalated with increasing stress levels, with the initial cycle at each level demonstrating the most pronounced irreversible deformation. At equivalent stress levels, the irreversible deformation exhibits a very consistent pattern for stress levels 1 and 2, excluding the initial cycle. At stress level 3, when the accumulated irreversible strain attains a certain threshold, the microcracks within the rock will progressively link and propagate. This results in an observable increase in activity over several cycles prior to failure, which can serve as a precursor to the damage of the specimen. The variation rule of cumulative irreversible deformation is shown in Figure 9. The cumulative irreversible deformation increases in a sloping manner. As the cyclic period accelerates, the cumulative plastic deformation gradually rises. Additionally, as the stress level increases, the gap between the accumulated irreversible deformations during each cyclic period widens progressively.

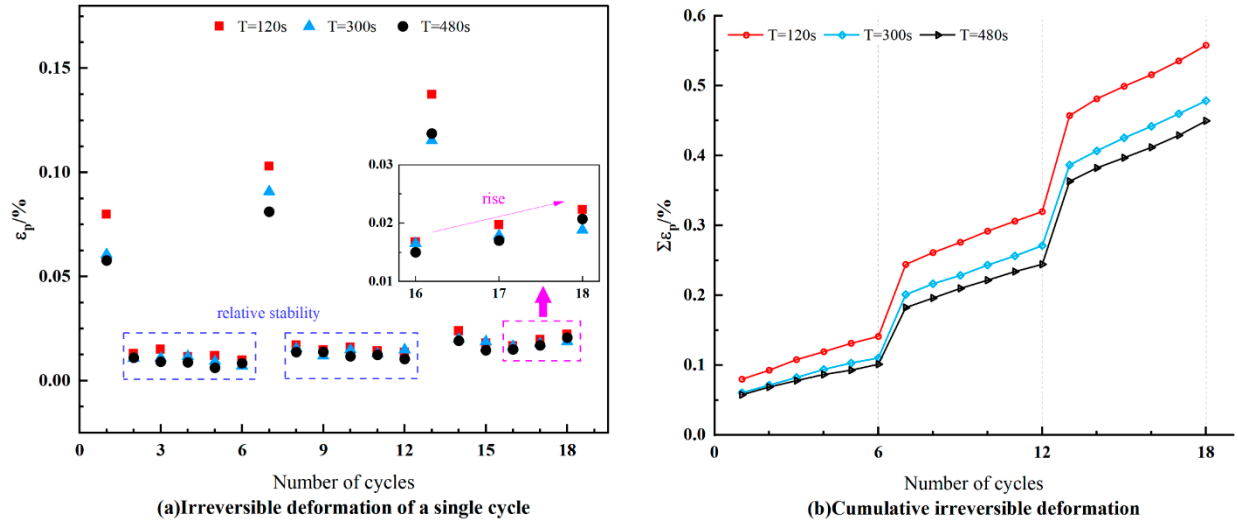


Figure 9. Curve of irreversible deformation with the number of cycles.

The linear fitting equations (in Table 1) allow us to express the relationship between cumulative irreversible deformation and the number of cycles at each stress level. It is observed that the rate of accumulation of irreversible deformation increases with higher stress levels. The rate of increase in cumulative irreversible deformation gradually accelerates as the cyclic period shortens under the same stress conditions. For stress level 1, the values of a at T = 120 s, 300 s, and 480 s are 0.012, 0.010, and 0.008, respectively. The results illustrate that a higher sensitivity to plastic deformation in coal samples, under conditions of high strain rate and high stress, is more likely to lead to structural deterioration and induce instability damage.

Table 1. Fitting equations for cumulative irreversible deformation versus number of cycles for each stress level.

T/s	Stress Level	Fitting Formula ($y = ax + b, 1 \leq x \leq 6$)	R^2
120	1	y = 0.069 + 0.012x	0.99
	2	y = 0.231 + 0.015x	0.99
	3	y = 0.439 + 0.019x	0.98
300	1	y = 0.051 + 0.010x	0.99
	2	y = 0.187 + 0.014x	0.98
	3	y = 0.369 + 0.018x	0.99
480	1	y = 0.051 + 0.008x	0.99
	2	y = 0.171 + 0.012x	0.99
	3	y = 0.346 + 0.017x	0.99

4.4. Damage Variable D_s

In order to characterize the degree of damage evolution in coal, Xie [36] defined damage variables based on the decay of elastic modulus:

$$D = 1 - \frac{\overline{E}}{E_0} \tag{6}$$

where $\overline{E}$ is the elastic modulus of the damaged rock, and E_0 is the elastic modulus of the rock when it is non-damaged. However, the above equation is only suitable for describing

the elastic damage behavior, and for the loading and unloading process of an elastic–plastic material like coal, the damage variables need to be corrected [32]:

$$D_s = 1 - (1 - \frac{\varepsilon_p}{\varepsilon})\frac{E_u}{E_0} \tag{7}$$

where ε and ε_p are the total strain and total plastic strain, respectively, and E_u and E_0 are the unloaded modulus and initial elastic modulus, respectively.

Figure 10 shows the evolution curve of the damage variable. Based on the rate of change of the damage variable D_S at each stress level, coal damage can be categorized into three stages: deceleration, stabilization, and acceleration. During the deceleration damage stage, the original defects are gradually compacted, the density of the internal structure is enhanced, and the damage caused by subsequent cycling continues to diminish. During the stabilization damage stage, the specimen is further compacted to enhance its mechanical properties. No new cracks or rupture surfaces have emerged, as the extent of plastic deformation is negligible, and the cumulative damage exhibits a relatively stable pattern of change. In the acceleration damage stage, the specimen is subjected to higher stress disturbances, causing cracks to continue closing, developing, and expanding under cyclic loading. The plastic deformation zone expands. Consequently, the damage within the specimen continues to increase, and the rate of increase accelerates.

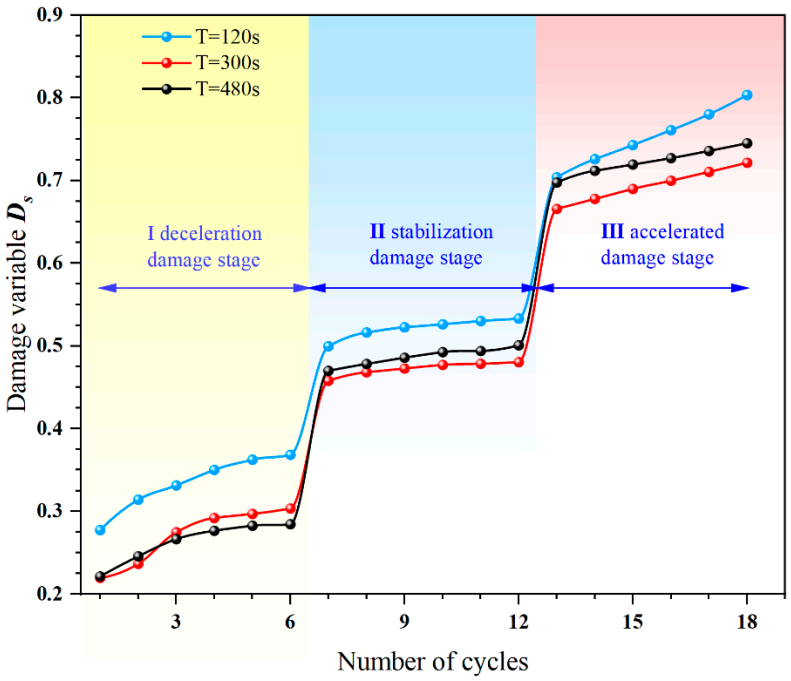


Figure 10. Curve of the damage variable *Ds*.

To compare the variation rules of D_S curves for coal samples with different cyclic periods, it can be observed that during the accelerated damage stage, the growth rates of D_S are 2.21%, 1.68%, and 1.23% at T = 120 s, 300 s, and 480 s, respectively. It indicates that under identical stress conditions, a shorter cyclic period results in a more rapid accumulation of damage in the specimen prior to imminent failure, thereby increasing the intensity of internal degradation.

5. Energy Characteristics

5.1. Energy Evolution

Assuming that there is no heat exchange during the deformation and destruction of the coal rock, then according to the first law of thermodynamics, the energy conversion follows the following equations [37].

$$U_i = U_{ei} + U_{di} \tag{8}$$

$$U_i = \int \sigma'_{1+} d\varepsilon_{1+} + 2\int \sigma'_{3+} d\varepsilon_{3+} \tag{9}$$

$$U_{ei} = \int \sigma'_{1-} d\varepsilon_{1-} + 2\int \sigma'_{3-} d\varepsilon_{3-} \tag{10}$$

The ratio of elastic and dissipated energy to the input energy is calculated and plotted separately in Figure 11. It has been observed that as stress levels increase, a sudden surge in energy occurs during the first cycle at each level. Overall, both the input energy and elastic energy increase incrementally. In comparison to the first two stress levels, the dissipated energy shows a significant increase. The input and elastic energies decrease with an increasing number of cycles at each stress level. The dissipated energy decreases with the number of cycles in the first two stress levels, but in stress level 3, it exhibits a pattern of initially decreasing followed by an increase.

To analyze the impact of stress levels on cumulative dissipated energy, we define the stress ratio as σ_1/σ_3. The cumulative dissipated energy exhibits a stepwise growth pattern throughout the entire process cycle. At stress levels 1 and 2, the relationship between cumulative dissipated energy and the number of cycles gradually transitions from a logarithmic to a linear pattern. The rate of growth of cumulative dissipated energy increases significantly compared to the previous two levels in stress level 3. The cumulative dissipated energy consistently increases throughout the final cycles preceding injury. The sensitivity of cumulative dissipated energy to the stress ratio was minimal when the stress ratio was below 3 and the cumulative dissipated energy markedly increased when the stress ratio surpassed 3. For instance, when the cyclic period T was 120 s, when the stress ratio reached 3.1, the cumulative dissipated energy increased rapidly to 26.87 MPa, which is approximately twice that of the stress ratios at the first two levels. This indicates that there is not a straightforward linear relationship between the stress ratio and the cumulative dissipated energy. When a specific stress ratio is reached, cracks within the coal body accelerate damage evolution and require more energy for crack initiation and effective expansion.

At the lower stress levels of the first two stages, the variation curve of the dissipated energy percentage with the number of cycles is in the shape of “L”, which first decreases and then stabilizes. This suggests that most of the energy is stored as elastic energy, while the dissipated energy correlates with the extent of crack closure due to compaction. Over time, the percentage of dissipated energy gradually decreases and stabilizes. In the highest stress levels, the new cracks generated start to evolve faster, the frictional slip between the rupture surfaces increases, and more energy is converted into dissipated energy. As a result, a greater amount of energy is converted into dissipated energy. The percentage of dissipated energy initially decreases, then stabilizes, and subsequently starts to increase, forming an approximate “U” shape.

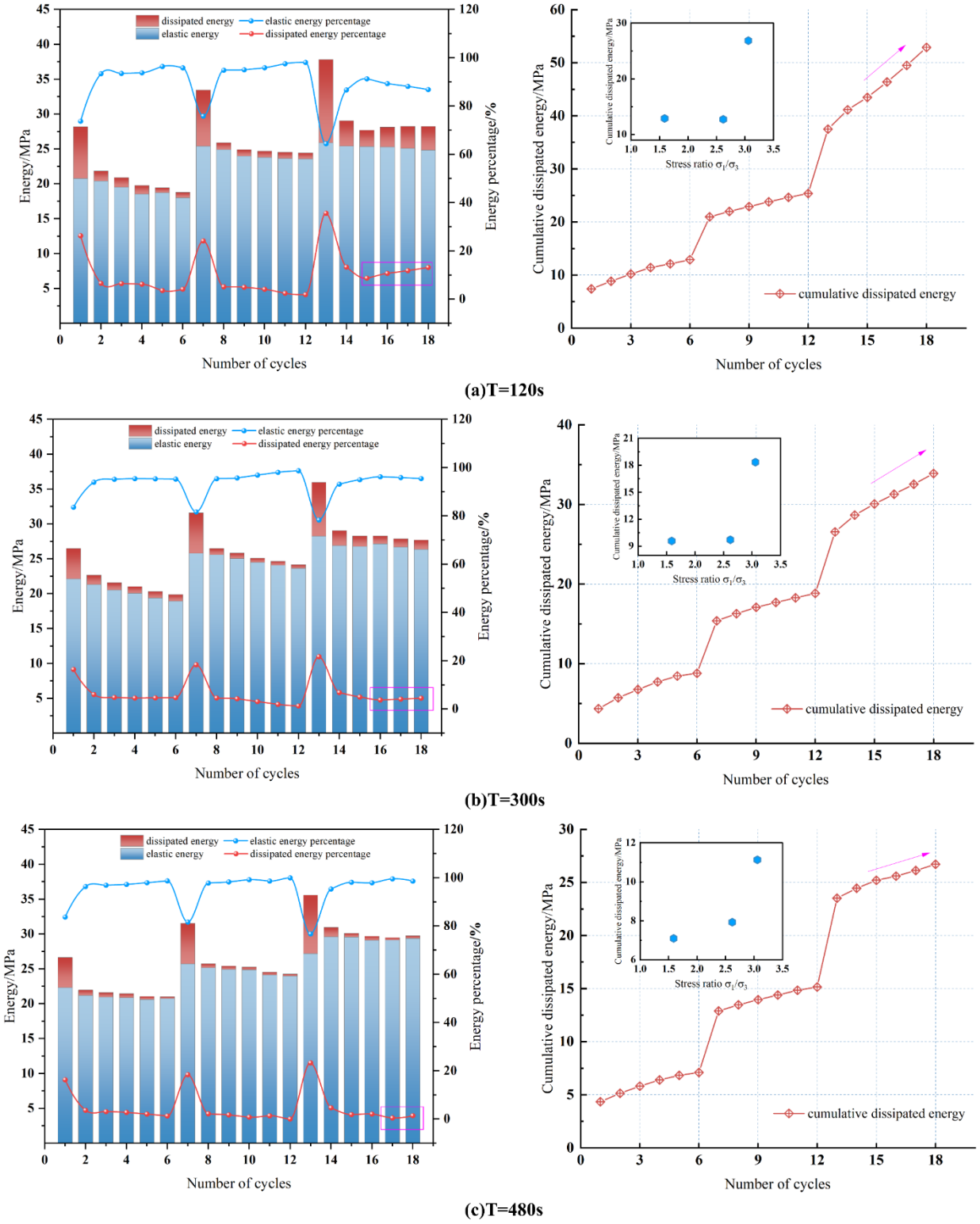


Figure 11. The evolution of energy indicators with the number of cycles.

Compared to the average dissipated energy share in each stress level under different cyclic periods, it can be found that the average dissipated energy percentage in each stress level of coal samples decreases with the increase in the cyclic period. For instance, in stress level 1, the downward magnitude is 22.75% and 29.30%, respectively. From Figure 12, it can be found that the cumulative dissipated energy decreases gradually with the increase in the cyclic period to 52.51 MPa, 37.66 MPa, and 25.89 MPa, respectively. The cumulative dissipated energy percentage decreases with the increase in the cyclic period, and its

percentage is 11.14%, 7.96%, and 5.49%, with downward magnitudes of 28.51% and 31.06%, respectively. Accordingly, the percentage of cumulative elastic energy increases gradually with cyclic period, and the ratio is in the range of 85% to 95%. The aforementioned results indicate that an increase in the cyclic period affects the energy distribution of the specimen, primarily evidenced by a reduction in dissipated energy. Additionally, the ratio of dissipated energy to input energy diminishes. This is mainly due to the fact that the deceleration of the loading rate primarily leads to a decrease in kinetic energy, diminishing the impact rupture effect on the specimen, prolonging the slip contact duration within the specimen, and augmenting the stored elastic energy.

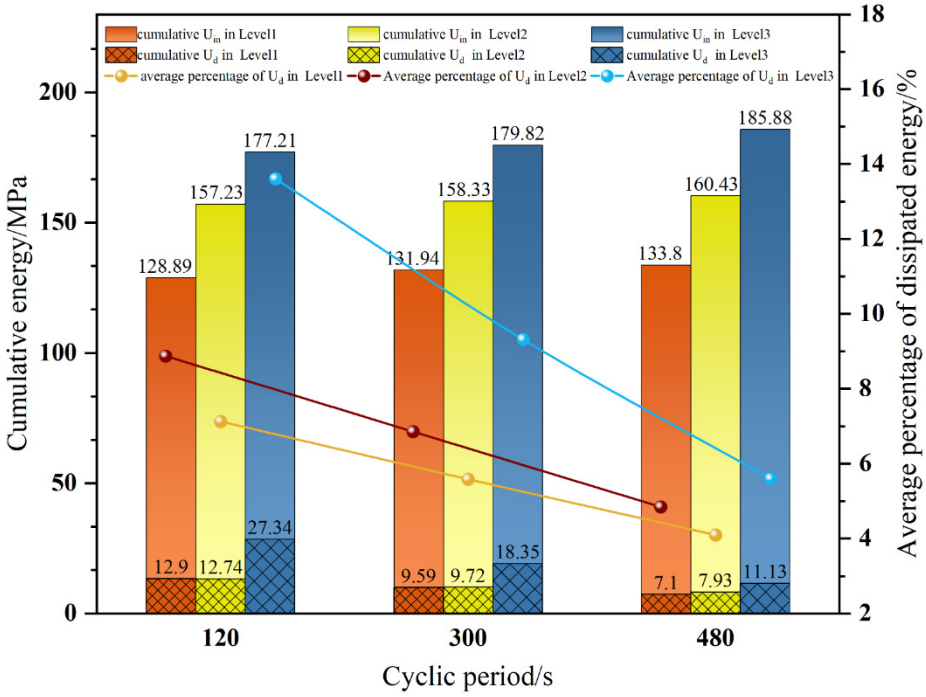


Figure 12. Energy comparison at different cyclic periods.

5.2. Damping Ratio

The damping ratio reflects the hysteresis of the rock during cyclic loading. It is caused by the internal friction effect during the deformation of the rock as well as the viscous consumption of energy by the fluid. The damping ratio λ is calculated by the following formula [31]:

$$\lambda = \frac{1}{\pi} \frac{A}{4A_s} \tag{11}$$

where A is the area of the hysteresis loop, and A_s is the area enclosed by the peak stress corresponding to the strain and the center of the ellipse.

Some scholars have modified the above equation from the energy point of view, based on the definition of damping ratio [32]:

$$\lambda_i = \frac{1}{\pi} \frac{U_{di}}{4U_{ei}} \tag{12}$$

where λ_i is the damping ratio of the ith cycle, U_{di} is the dissipated energy of the ith cycle, and U_{ei} is the elastic strain energy of the ith cycle.

From Figure 13, it can be noticed that there is a sudden increase in the damping ratio of the first cycle of each level under each cyclic period. The damping ratios of the other cycles fluctuated between 0 and 0.5, showing a trend of decreasing and then rebounding with the increase in the stress level, and the degree of fluctuation of the damping ratio of the

final level was greater than that of the first two levels; for example, the average damping ratios of the specimen with a cyclic period of 120 s were 0.02, 0.01, and 0.03 at each stress level, respectively. Analyzing the same stress level, the viscous interactions of the particle structures diminish upon compaction of the specimen, leading to a decrease in the energy dissipated via damping. At stress level 2, the effect of viscous forces between the mineral particles is not significant, and the damping ratio maintains a relatively stable decreasing trend. At stress level 3, the fatigue damage condition of the specimen is aggravated, and the energy consumption caused by the viscous damping effect when the crack expands is more obvious, which makes the damping ratio increase at the later stage.

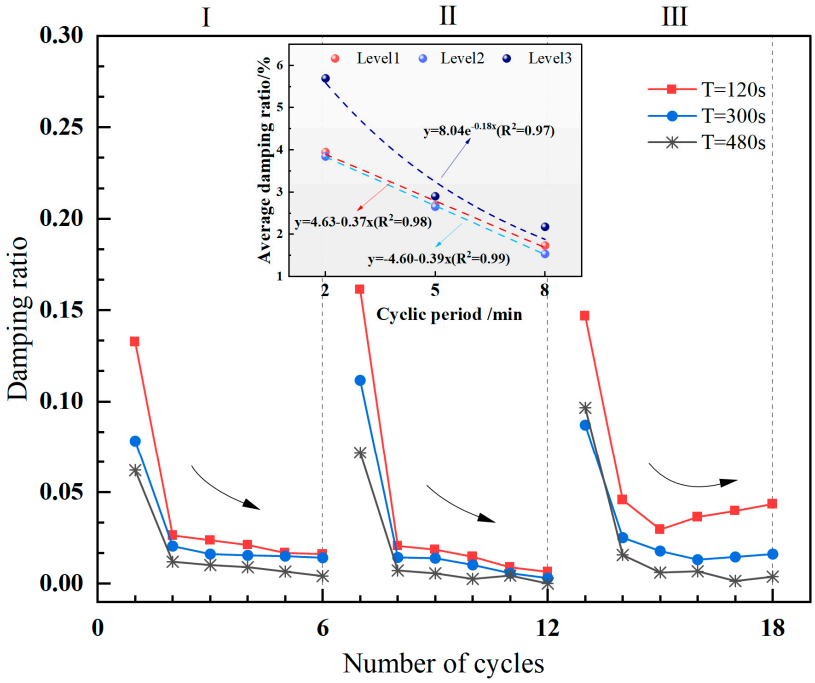


Figure 13. Change curve of damping ratio.

The damping ratios at different cyclic periods were analyzed, and it was found that the acceleration of the cyclic period increased the damping ratio of the specimens under the same stress conditions. The variation of the average damping ratio with a cyclic period in each stress level is shown in Figure 13. The relationship between the average damping ratio and the cyclic period satisfies a linear variation when in stress levels 1 and 2 and then changes to an exponential relationship in stress level 3. The average damping ratios of each stress level except the first cycle were analyzed, and the average damping ratios at stress level 1 were 0.021, 0.016, and 0.008 for the cyclic periods of 120 s, 300 s, and 480 s, respectively, with changes of 23.81% and 50.00%. At stress level 2, the average damping ratios were 0.014, 0.009, and 0.004, respectively, with changes of 35.71% and 55.56%; and at stress level 3, the average damping ratios were 0.033, 0.013, and 0.007, respectively, with changes of 60.61% and 46.15%. This may be due to the rapid loading and unloading of bias stresses that weaken the microstructural stability and increase the misalignment friction between the mineral particles, while the crack extension zone is subjected to a greater impact force and the presence of a relatively large number of coal fragments and particles between interfaces, leading to a relative increase in the energy used to overcome the damping force.

5.3. Damage Variable D_d

Through the above analysis of the energy evolution of coal samples in the cyclic loading and unloading process, it can be assumed that the dissipated energy is the intrinsic cause of the damage of coal samples, and this paper reacts to the damage characteristics of coal samples in the cyclic process through the variable of cumulative dissipated energy, and the formula of the damage variable, according to the definition of rock damage, is as follows [38]:

$$D_d = \frac{\sum U_{di}}{U_{dc}} \tag{13}$$

where U_{dc} is the dissipated energy accumulated when the specimen reaches peak strength.

According to the accumulative rate of the damage variable D_d curve in Figure 14, the damage process of coal samples in this test can also be divided into three stages of "deceleration–stabilization–acceleration" damage. During the deceleration damage phase, the first cycle produced about 10% damage, and the dissipated energy due to the density effect continues to increase but at a reduced rate during subsequent cycles. During the stabilization damage stage, the elastic properties of the specimen are enhanced at this stage, the microcracks have not formed significant expansion and connection, and less energy is dissipated; the final accumulation of damage is about 40%. In the acceleration damage stage, the structure of the specimen gradually shifted from stability to rupture with the deterioration of the load-bearing properties, the cyclic loading exacerbated the damage evolution of the cracks, and more energy is consumed for each cycle, with the damage rapidly accumulating. Eventually, the damage accumulation reaches about 80%. In the accelerated damage stage, the average growth rates of the damage variable D_d were 6.97%, 5.51%, and 2.63% under the cyclic periods of 120 s, 300 s, and 480 s, respectively, and it can similarly be found that the damage growth rate of the specimen increases with the accelerated cyclic period, and the degree of internal damage evolution is more drastic.

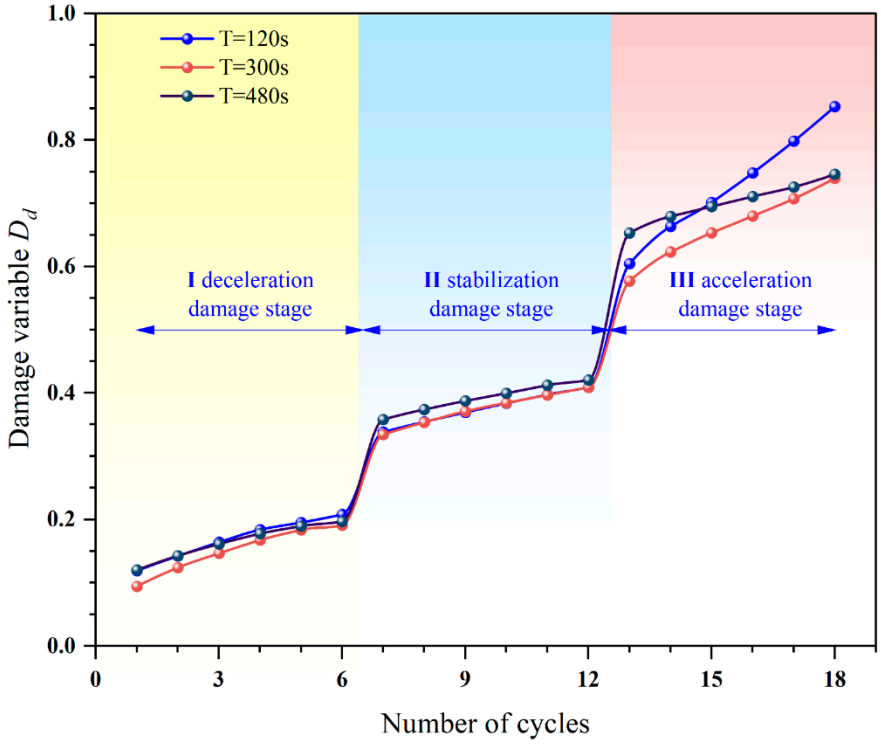


Figure 14. Curve of the damage variable D_d.

6. Conclusions

(1) With the increase in stress level, the shape of the axial hysteresis loop of the specimen changes from the "shuttle" type to the "streamline" type, and the shape of the annular hysteresis loop mainly shows an elastic effect, which is of the "streamline" type. The shape of the loop direction hysteresis loop mainly shows the elastic effect, and both of them are of the "streamline" type. With the increase in the cyclic period, due to the slowing down of the loading rate, the structural stability of the specimen at the cyclic unloading place is enhanced, the angle of the stress–strain curve at the partial stress unloading place is gradually increased, and the elastic response sensitivity is changed from an "obtuse angle" to an "acute angle". The sensitivity of the elastic response is enhanced.

(2) The elastic modulus decreases step by step with the number of cycles in a "increase–stabilization–decline" pattern. The Poisson's ratio rises incrementally with increasing stress levels, and the gradual elevation of Poisson's ratio over several cycles prior to damage might be considered a forerunner to the destabilization of coal rock. This is due to the increase in shear stress that intensifies the specimen's internal crack development and expansion behavior, along with the stiffness of the coal specimen and its resistance to deformation. As the cyclic period accelerates, the elastic modulus decreases and the Poisson's ratio increases, which is due to the faster loading rate resulting in increased frictional slip between particles within the coal sample and the increased radial expansion of the specimen.

(3) The cumulative irreversible deformation increases, step by step, with the number of cycles in a slope-like manner. Faster cycle periods have a greater impact on the specimen, intensify joint and fracture development, and increase the irreversible deformation of coals. According to the damage variable, D_s, defined by the deformation parameter, the test process can be divided into three stages of "deceleration–stabilization–acceleration" according to the rate of change, and in the accelerated accumulation stage, the rate of damage accumulation accelerates with the cyclic period.

(4) The cumulative dissipated energy increases stepwise with the number of cycles, and in the last few cycles, the cumulative dissipated energy increases gradually due to the continuous expansion of the plastic damage zone, and the cumulative dissipated energy increases significantly when the stress ratio is greater than 3. The majority of the input energy in each cycle is conserved as elastic energy, with the dissipated energy ratio resembling a "L" shape at stress levels 1 and 2. At stress level 3, due to the rapid propagation of cracks, the dissipated energy ratio takes on a "U" shape and evidently increases. As the cyclic period increases, the kinetic damage and friction-slip effects on the specimens diminish, resulting in a drop in the average dissipated energy ratio at each stress level.

(5) The relationship between the damping ratio and the number of cycles resembles the proportion of dissipative energy. The rapid loading and unloading during the cyclic period exacerbates misalignment friction, resulting in a greater impact force on the crack extension area. Additionally, the presence of increased coal debris between the interfaces enhances the specimen's damping characteristics. Consequently, the relationship between the average damping ratio and the cyclic period evolves into an exponential form as the stress level rises. The damage variable, D_d, defined based on the cumulative dissipated energy, can also characterize the three damage stages of the specimen under cyclic loading conditions.

Author Contributions: Conceptualization, Y.J.; methodology, X.Y. and D.Z.; writing—original draft preparation, Y.J. and X.M.; writing—review and editing, Y.J.; visualization, X.Y.; supervision, Y.J. All authors have read and agreed to the published version of the manuscript.

Funding: This work was funded by Jiangxi Provincial Thousand Talents Plan Project (jxsq 2019102082).

Institutional Review Board Statement: Not applicable.

Informed Consent Statement: Not applicable.

Data Availability Statement: The raw data supporting the conclusions of this article will be made available by the authors on request.

Conflicts of Interest: The authors declare no competing interests.

References

1. Ray, S.K.; Sarkar, M.; Singh, T.N. Singh Effect of cyclic loading and strain rate on the mechanical behaviour of sandstone. *Int. J. Rock. Mech. Min.* **1999**, *36*, 543–549. [CrossRef]
2. Hongpu, K.; Guofa, W.; Pengfei, J.; Jiachen, W.; Nong, Z. Conception for strata control and intelligent mining technology in deepcoal mines with depth more than 1000 m. *J. China Coal Soc.* **2018**, *43*, 1789–1800.
3. Liang, Y.; Junhua, X.; Nong, Z.; Ping, L. Development orientation and status of key technology for mine underground coal bed methane drainage as well as coal and gas simultaneous mining. *Chin. Coal Sci. Technol.* **2013**, *41*, 6–11.
4. Bagde, M.N.; Petroš, V. Fatigue properties of intact sandstone samples subjected to dynamic uniaxial cyclical loading. *Int. J. Rock. Mech. Min.* **2005**, *42*, 237–250. [CrossRef]
5. Bagde, M.N.; Petroš, V. Waveform effect on fatigue properties of intact sandstone in uniaxial cyclical loading. *Rock. Mech. Rock. Eng.* **2005**, *38*, 169–196. [CrossRef]
6. Bao, H.; Pei, R.; Lan, H.; Yan, C.; Xu, J.; Zhai, Y.; Xu, X. Damage evolution of Biotite quartz schist caused by mineral directional arrangement under cyclic loading and unloading. *Chin. J. Rock. Mech. Eng.* **2021**, *40*, 2015–2026.
7. Wang, H.; Xu, W.; Cai, M.; Xiang, Z.; Kong, Q. Gas permeability and porosity evolution of a porous sandstone under repeated loading and unloading conditions. *Rock. Mech. Rock. Eng.* **2017**, *50*, 2071–2083. [CrossRef]
8. Wang, J.; Liu, M.; Jian, F.; Chai, H. Mechanical behaviors of a sandstone and mudstone under loading and unloading conditions. *Environ. Earth Sci.* **2019**, *78*, 30. [CrossRef]
9. Xiao, W.; Yu, G.; Li, H.; Zhan, W.; Zhang, D. Experimental study on the failure process of sandstone subjected to cyclic loading and unloading after high temperature treatment. *Eng. Geol.* **2021**, *293*, 106305. [CrossRef]
10. Zhu, Z.; Tian, H.; Kempka, T.; Jiang, G.; Dou, B.; Mei, G. Mechanical behaviors of granite after thermal treatment under loading and unloading conditions. *Nat. Resour. Res.* **2021**, *30*, 2733–2752. [CrossRef]
11. Wei, Y.-L.; Yang, C.-H.; Guo, Y.; Liu, W.; Wang, L.; Heng, S. Experimental investigation on deformation and fracture characteristies ofbrittle shale with natural cracks under uniaxial cyclic loading. *Rock. Soil Mech.* **2015**, *37*, 1649–1658.
12. Yang, S.; Tao, Y.; Tang, J. Experimental study of triaxial strength and deformation of single jointed sandstone under cyclic loading. *J. China Univ. Min. Technol.* **2020**, *49*, 819–825.
13. Dang, S.; Bi, J.; Zhao, Y.; Wang, C.; Li, J.; Hu, H. Strain evolution and fatigue damage characteristics analysis of sandstones during multi-level triaxial cyclic loading and unloading under varying stress limits. *Rock. Mech. Rock. Eng.* **2023**, *56*, 2649–2671. [CrossRef]
14. Kang, P.; Jiaqi, Z.; Quanle, Z.; Junhui, M. Fatigue deformation characteristics and damage model of sandstones subjected to cyclic Loading: Implications for fatigue life prediction. *Int. J. Geomech.* **2022**, *22*, 04021261. [CrossRef]
15. Yu, J.; Liu, Z.H.; Lin, L.H.; Huang, J.G.; Ren, W.B.; Zhou, L. Characteristics of dilatancy of marble under variable amplitude cyclic loading and unloading. *Rock. Soil Mech.* **2021**, *42*, 2934–2942.
16. Ren, J.X.; Yun, M.C.; Zhang, K.; Jing, S. Experimental research on coal and rock strength deterioration under combined static and dynamic triaxial loading. *Chin. Coal Sci. Technol.* **2021**, *49*, 105–111.
17. Wang, R.; Wei, C.; Liu, J.; Li, Z.; Tan, Y.H. Macro and micro characteristics of jointed sandstone under cyclic loading and unloading. *Chin. J. Rock. Mech. Eng.* **2023**, *42*, 810–820.
18. Chen, Y.; Zuo, J.; Li, Z.; Dou, R. Experimental investigation on the crack propagation behaviors of sandstone under different loading and unloading conditions. *Int. J. Rock. Mech. Min.* **2020**, *130*, 104310. [CrossRef]
19. Duan, M.; Jiang, C.; Xing, H.; Zhang, D.; Peng, K.; Zhang, W. Study on damage of coal based on permeability and load-unload response ratio under tiered cyclic loading. *Arab. J. Geosci.* **2020**, *13*, 250. [CrossRef]
20. Gong, F.Q.; Wu, C.; Luo, S.; Yan, J.Y. Load–unload response ratio characteristics of rock materials and their application in prediction of rockburst proneness. *Bull. Eng. Geol. Environ.* **2019**, *78*, 5445–5466. [CrossRef]

21. Duan, M.; Lu, M.; Ban, R.; Yang, K.; Lyu, X.; Jiang, C.; Hu, X.; Tang, J. Study on the failure and acoustic emission characteristics of coal under graded cyclic loading and unloading stress paths. *Sci. Rep.* **2024**, *14*, 26863. [CrossRef] [PubMed]
22. Li, Y.; Zhang, S.; Wen, Z.; Zhao, R.; Cao, Z. Energy conversion and fragment distribution characteristics of coal sample under uniaxial cyclic loading. *J. China Coal Soc.* **2019**, *44*, 1411–1420.
23. Han, C.; Pang, D.P.; Li, D.J. Analysis of energy evolution during the step loading and unloading creepexperiments of sandstone. *Rock. Soil Mech.* **2020**, *41*, 1179–1188.
24. Yang, Z.; Zhu, W.; Guan, K.; Yan, B.; Jia, H. Influence of dynamic disturbance on rock creep from time, space and energy aspects. *Genmat. Nat. Hazards Risk* **2022**, *13*, 1065–1086. [CrossRef]
25. Zuo, J.; Chen, Y.; Song, H. Study progress of failure behaviors and nonlinear model of deep coal-rock combined body. *J. Cent. South Univ. (Sci. Technol.)* **2021**, *52*, 2510–2521.
26. Liu, Z.; Wang, W.; Luo, J.A.; Miao, G. Method of energy evolution of rock under uniaxial compression test. *China Coal Soc.* **2020**, *45*, 3131–3139. [CrossRef]
27. Zhang, B.W.; Fang, K.; Wang, C.; Zhao, T.B.; Zhang, X.F. Energy evolution characteristics of rock under different confining conditions. *Front. Earth Sci.* **2022**, *10*, 886134. [CrossRef]
28. Xu, H.; Rong, C.; Wang, B.; Zhang, Q.; Shen, Z.; Jin, Y. Dynamic mechanical behavior and energy dissipation characteristics of low-temperature saturated granite under cyclic impact loading. *Sci. Rep.* **2024**, *14*, 26840. [CrossRef]
29. Song, H.; Zhao, Y.; Wu, Y.; Li, X.; Gong, Z.; Sun, Z.; Jiang, Y.; Guo, Z. Effect of water on the damage and energy dissipation feature of coal under uniaxial cyclic loading–unloading condition. *Energy Sci. Eng.* **2023**, *11*, 4092–4107. [CrossRef]
30. He, M.M.; Pang, F.; Wang, H.T.; Zhu, J.W.; Chen, Y.S. Energy dissipation-based method for strength determination of rock under uniaxial compression. *Shock Vib.* **2020**, *2020*, 8865958. [CrossRef]
31. Zhang, L.M.; Gao, S.; Wang, Z.Q.; Cong, Y. Analysis of marble failure energy evolution under loading and unloading conditions. *Chin. J. Rock. Mech. Eng.* **2013**, *32*, 1572–1578.
32. Jiang, C.B.; Wei, C.; Zhuang, W.J.; Duan, M.K.; Chen, Y.F.; Yu, T. Research on deformation characteristics and energy evolution mechanisms ofshale under constant amplitude cyclic loading. *Chin. J. Rock. Mech. Eng.* **2020**, *39*, 2416–2428.
33. Jiang, C.; Li, Z.; Wang, W.; Wen, Z.; Duan, M.; Geng, W. Experimental investigation of the mechanical characteristics and energy dissipation of gas-containing coal under incremental tiered cyclic loading. *Geomech. Geophys. Geo-Energy Geo-Resour.* **2021**, *7*, 75. [CrossRef]
34. Meng, Q.B.; Wang, C.K.; Huang, B.X.; Pu, H.; Zhang, Z.Z.; Sun, W.; Wang, J. Rock energy evolution and distribution law under triaxial cyclic loading and unloading conditions. *Chin. J. Rock. Mech. Eng.* **2020**, *39*, 2047–2059.
35. Yu, B.; Zhang, D.; Li, S.; Xu, B.; Liu, C.; Liu, Y. Biot's coefficient and permeability evolution of damaged anisotropic coal subjected to true triaxial stress. *Rock. Mech. Rock. Eng.* **2023**, *56*, 237–260. [CrossRef]
36. Xie, H.P.; Ju, Y.; Li, L.Y.; Peng, R.D. Energy mechanism of deformation and failure of rock masses. *Chin. J. Rock. Mech. Eng.* **2008**, *27*, 1729–1740.
37. Zhang, A.; Xie, H.; Zhang, R.; Gao, M.; Xie, J.; Jia, Z.; Ren, L.; Zhang, Z. Mechanical properties and energy characteristics of coal at different depths under cyclic triaxial loading and unloading. *Int. J. Rock. Mech. Min.* **2023**, *161*, 105271. [CrossRef]
38. Chen, Y.; Guo, W.; Zuo, J.; Heng, S.; Dou, R. Effect of triaxial loading and unloading on crack propagation and damage behaviors of sandstone: An experimental study. *Rock. Mech. Rock. Eng.* **2021**, *54*, 6077–6090. [CrossRef]

Disclaimer/Publisher's Note: The statements, opinions and data contained in all publications are solely those of the individual author(s) and contributor(s) and not of MDPI and/or the editor(s). MDPI and/or the editor(s) disclaim responsibility for any injury to people or property resulting from any ideas, methods, instructions or products referred to in the content.